

AnimateAnything: Fine-Grained Open Domain Image Animation with Motion Guidance

Zuozhuo Dai , Zhenghao Zhang , Yao Yao , Bingxue Qiu , Siyu Zhu , Long Qin , Weizhi Wang
Alibaba Group

Abstract

Image animation is a key task in computer vision which aims to generate dynamic visual content from a static image. Recent image animation methods employ neural based rendering technique to generate realistic animations. Despite these advancements, achieving fine-grained and controllable image animation guided by text remains challenging, particularly for open-domain images captured in diverse real environments. In this paper, we introduce an open domain image animation method that leverages the motion prior of video diffusion model. Our approach introduces targeted motion area guidance and motion strength guidance, enabling precise control the movable area and its motion speed. This results in enhanced alignment between the animated visual elements and the prompting text, thereby facilitating a fine-grained and interactive animation generation process for intricate motion sequences. We validate the effectiveness of our method through rigorous experiments on an open-domain dataset, with the results showcasing its superior performance. Project page can be found at <https://animationai.github.io/AnimateAnything>.

1. Introduction

The field of image animation has recently gained attention, especially for creating short videos and animated GIFs for social media and photo-sharing platforms. However, current image animation methods [3, 9, 18, 28, 33, 34] are limited in animating specific object types, such as fluid [18, 28, 33, 34, 38], natural scenes [7, 23, 29, 46, 59], human hair [58], portraits [12, 53, 54], and bodies [3, 4, 25, 47, 54, 55], limiting their practical application in open domain scenarios. Recent advancements in video diffusion models [11, 14, 17, 26, 32, 48, 52, 65] have enabled the generation of diverse and realistic videos based on reference texts and images. In this paper, we aim to address the open domain image animation problem by leveraging the motion priors of video diffusion models. We propose a controllable diffusion-based image animation method capable of animating arbitrary objects within an image while pre-

serving their details. Our practical experience has shown that creating animations solely through prompt text is laborious and challenging, and results in limited control over finer details. To enhance user control over the animation process, we introduce the motion area guidance and motion strength guidance, allowing for precise and interactive control of the motion speed of multiple objects, significantly improving controllable and fine-grained image animation.

To accurately identify movable objects and their corresponding movable regions within an image, we introduce motion area masks. Inspired by ControlNet [63], we append the mask along the channel dimension of the video latent representation and initialize the convolutional weights to zero, allowing them to adjust incrementally during the training process. This approach enables fine-grained and precise control over multiple movable areas in the input image, even when using multiple prompting texts. Training the model to follow the guidance of the motion area mask presents a significant challenge, as it is difficult to amass and annotate a substantial corpus of real videos in which only specific regions are in motion. To address this issue, we propose an unsupervised technique to generate synthetic videos with motion area masks derived from actual videos. The model is trained on both synthetic and real videos to ensure the generation of realistic videos directed by the motion area mask.

To effectively control the speed of moving objects in image animation, we introduce the metric of motion strength. Frame rate per second (FPS) represents the number of frames displayed in one second and previous methods [5, 21, 52] relied on FPS to control motion speed. However, it is important to note that different object types may exhibit varying motion speeds, and FPS primarily serves as a global scaling factor to indirectly adjust the motion speed of multiple objects. For instance, a video featuring a sculpture may have a high FPS but zero motion speed. To enable direct learning of motion speed by the video diffusion model, we propose a novel motion strength loss to supervise the model in learning inter-frame variances in the latent space.

In recent developments, image-to-video diffusion models [5, 17, 52] have emerged for generating realistic videos

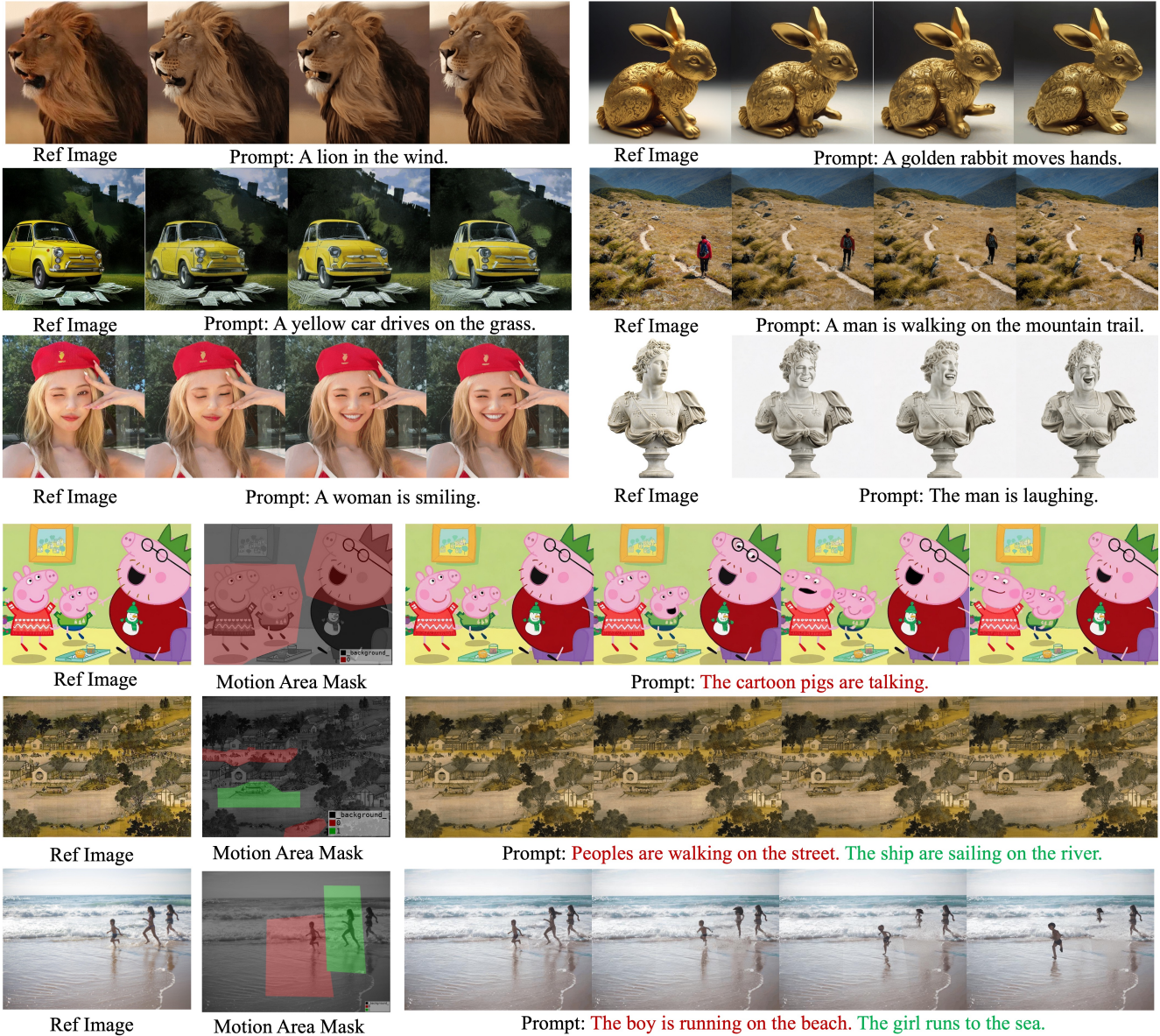


Figure 1. Examples of our method for image animation. The first three rows illustrate the use of prompt text to animate the reference image, with the 6th, 11th, and 16th frames of the generated animation visualized. The last three rows demonstrate the precise control of movable objects using motion mask guidance in images containing multiple objects. The last two rows show the iterative generation of animation using red and green prompts to animate objects in the corresponding masks. Additional examples are provided in the supplemental material.

from input images. These models employ the CLIP vision encoder [41] to encode the reference image, capturing its semantic structure and style. However, they often struggle to preserve fine-grained visual details of the reference image. To address this limitation and apply video diffusion models to image animation tasks, we propose encoding the reference image into a latent space using a VAE [27]. This latent representation can then serve as the first frame of the generated video, effectively preserving image details without introducing additional parameters to existing video diffusion models, thereby enabling efficient training and inference for

image animation tasks.

The combination of prompt text, motion area mask, and motion strength guidance enables the generation of complex image animations in diverse real-world scenarios. A sequential approach can be adopted, where a specific object is initially animated with a prompt text, followed by the animation of another object with a different prompt text. This iterative process allows users to progressively and interactively modify the image animation until a satisfactory outcome is achieved. An example of interactive image animation is illustrated in the last row of Figure 1. Initially,

the actions of the boy are manipulated using a motion area mask marked in red together with the prompting text: “the boy is running on the beach”. Subsequently, one of the two girls is animated through another motion area mask marked in green, accompanied by the prompting text: “the girl runs to the sea”. In summary, our contributions in this work are threefold:

- We introduce a highly flexible motion guidance mechanism that allows for fine-grained open domain image animation guided by motion area and motion strength. We propose a synthetic motion area mask generation method and a novel motion strength loss for effective training.
- Our image animation framework supports combined guidance from text, motion area, and motion strength, enabling an interactive animation generation process for creating complex animations.
- By enhancing the image guidance mechanism of the current video diffusion model, we achieve a state-of-the-art FVD score of 443 on the zero-shot MSRVTT dataset.

2. Related Work

2.1. Image Animation

Image animation involves creating a video sequence from a static image. Initial approaches manually simulated motion for specific object types, such as mass simulation for vegetation and 2D rigid transformations for inanimate objects [8, 23]. Later research predicted inter-frame flows and utilized neural rendering to produce cinemagraphs, primarily focusing on fluid dynamics [18, 28, 33, 34, 38], natural environments [7, 23, 29, 46, 59], and human features such as hair [58], faces [12, 53, 54], and body movements [3, 4, 25, 47, 54, 55]. Recent advancements have seen diffusion-based models that generate diverse video content guided by a still image. The Make-it-move framework [20] captures motion patterns through motion anchors, which are then used to condition a VQ-VAE model. Despite its innovation, the model is limited by its dependency on the specific motion-object pairs from the training data, restricting its efficacy on open-domain images. The LFDm model [36] adopts a two-stage process for human-centric video generation, while Generative Dynamics [29] focuses on modeling oscillatory motion in natural scenes. However, these methods are domain-specific. In contrast, our approach addresses the challenge of open-domain image animation.

2.2. Image generation with diffusion models

The evolution of image generation research has transitioned from traditional frameworks such as Generative Adversarial Networks (GANs) [13], Variational Autoencoders (VAEs) [27], and autoregressive transformer models (ARMs) [6], to the more recent diffusion models (DMs) [15]. This shift is attributed to the stability, superior sample quality,

and conditional generation capabilities of DMs. DALLE-2 [42] represents a significant advancement by integrating the CLIP model [41] for text-image feature alignment, enabling text-prompted image synthesis. GLIDE [37] introduces classifier-free guidance to refine image quality, while Imagen [45] utilizes a sequence of diffusion models for high-resolution image creation. Latent Diffusion Models (LDMs) [42] employ an autoencoder [10] to manage the diffusion process in latent space, enhancing efficiency. Subsequent models like DiTs [39] and SDXL [40] further concentrate on latent space manipulation. For conditional generation, T2I-Adapter [35] and ControlNet [63] have been developed to integrate spatial conditions such as depth maps and sketches into LDMs. Composer [22] extends this by training LDMs with multiple conditions for more precise control. Building on these developments, our work introduces motion area and motion strength guidance to provide fine-grained control of image animation.

2.3. Video generation with diffusion models

Recent advancements in diffusion models (DMs) have shown great promise in video generation [37, 39, 40, 43, 45]. The Video Diffusion Model (VDM) [17] pioneers this domain by adapting the image diffusion U-Net architecture [44] into a 3D U-Net structure for joint image and video training. Imagen Video [16] employs a series of video diffusion models for high-resolution, temporally coherent video synthesis. Make-A-Video [48] innovatively learns motion patterns from unlabeled video data, while Tune-A-Video [57] explores one-shot video generation by fine-tuning LDMs with a single text-video pair. Text2Video-Zero [26] tackles zero-shot video generation using pretrained LDMs without further training. ControlVideo [64] introduces a hierarchical sampler and memory-efficient framework to craft extended videos swiftly. Concurrently, VideoCrafter1 [5] integrates image guidance from CLIP into diffusion models via cross-attention. Despite these innovations, capturing complex motion and camera dynamics remains challenging. VideoComposer [52] and DragNUWA [62] propose motion trajectory-based control for video generation, yet they fall short in interactive animation with multiple objects. Our approach addresses this by incorporating motion masks and motion strength parameters to precisely manipulate individual objects within an image, thus facilitating more user-centric interactive animation generation.

3. Method

We provide an overview of the video diffusion model in Section 3.1, followed by its adaptation for the image animation task in Section 3.2. Sections 3.3 and 3.4 offer detailed information on the integration of motion guidance into the generation process. Lastly, Sections 3.5 and 3.6 present the inference process under different guidance.

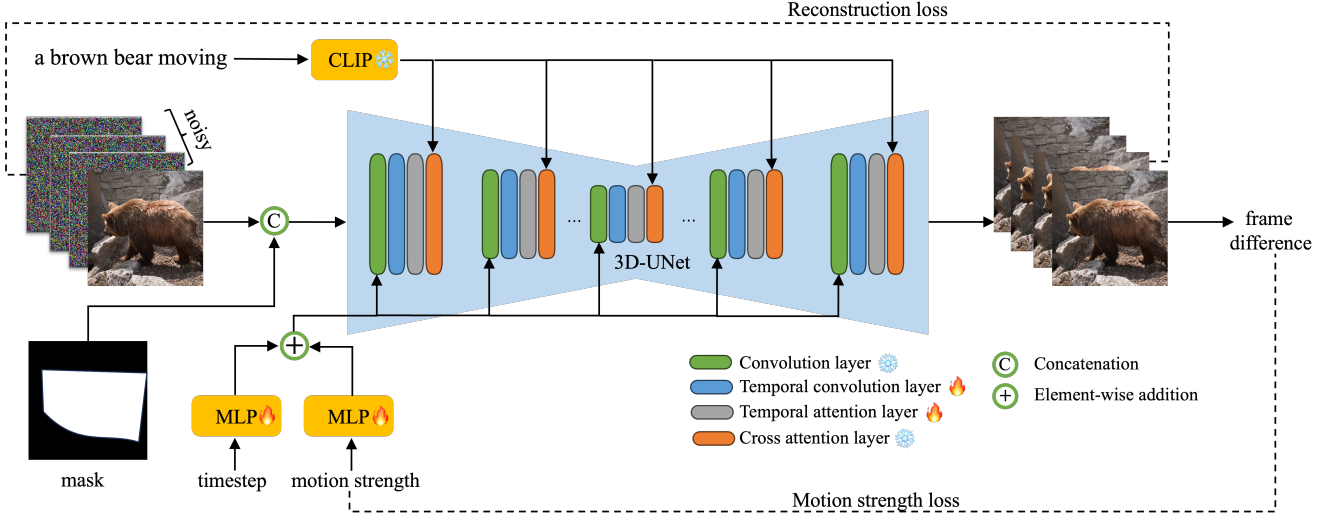


Figure 2. Overview of our pipeline. We adopt the widely used 3D U-Net based video diffusion model [11, 52] for image animation. Given a noisy video latent with shape (frames, height, width, channel), we concatenate the clean latent of the reference image and the noisy frames in the temporal dimension. Additionally, we concatenate the motion area mask with the video latent in the channel dimension. This results in the input latent with shape (frames+1, height, width, channel+1) for the 3D U-Net. To control the motion strength of the generated video, we project the motion strength as positional embedding and concatenate it with the time step embedding.

3.1. Background

In this section, we introduce the preliminary knowledge of the latent diffusion-based model (LDM) [43]. Given an image sample $x_0 \in \mathbb{R}^{3 \times H \times W}$, the LDM initially utilizes a pre-trained VAE to encode x_0 into a down-scaled latent representation $z_0 \in \mathbb{R}^{c \times h \times w}$. The forward process of the LDM can be described as a Markov chain that incrementally introduces Gaussian noise to the latent representation:

$$q(z_t|z_{t-1}) = \mathcal{N}(z_t; \sqrt{1 - \beta_t}z_{t-1}, \beta_t I), \quad (1)$$

where $t = 1, \dots, T$ and T denotes the total number of timesteps. β_t is a coefficient that controls the noise strength in step t . The iterative noise adding can be simplified as:

$$z_t = \sqrt{\bar{\alpha}_t}z_0 + \sqrt{1 - \bar{\alpha}_t}\epsilon, \quad \epsilon \sim \mathcal{N}(0, I), \quad (2)$$

where $\bar{\alpha}_t = \prod_{i=1}^t (1 - \beta_i)$. During training, the LDM learns the latent space distribution of the real data by predicting the noise ϵ added on z_t , resulting in a reduction of computational complexity for diffusion models. The objective function can be written as:

$$l_\epsilon = \|\epsilon - \epsilon_\theta(z_t, t, c)\|_2^2, \quad (3)$$

where $\epsilon_\theta(\cdot)$ denotes the noise prediction function of diffusion models, which is implemented by an U-Net [44] architecture. To control the generation process flexibly, LDM employs a domain-specific encoder to map the user-input condition c into an intermediate representation, which is then injected into the UNet via a cross-attention layer.

Video diffusion models [11, 17, 48, 52] expand upon the image LDM by incorporating a 3D U-Net, enabling them to effectively handle video data. The 3D U-Net incorporates an extra temporal convolution following each spatial convolution and a temporal attention block following each spatial attention block. To inherit the generation capacity from image data, the 3D U-Net is trained concurrently with both image and video data.

3.2. Image Animation with Video Diffusion Model

We employ the LDM VAE [43] to encode the reference image into a latent representation, denoted as z_{ref} , in order to retain more appearance details. The VAE is trained for image reconstruction, thus z_{ref} contains rich low-level image features. Although it may contain less semantic information compared to CLIP [41] vision tokens, the diffusion model itself has demonstrated powerful semantic understanding capabilities in tasks such as semantic segmentation [24, 30]. As illustrated in Figure 2, our training pipeline uses the reference image as the initial frame and adopts an auto-regressive strategy to forecast subsequent frames, facilitating image animation without extra model parameters. The first frame’s content is propagated to later frames via temporal convolution and attention mechanisms. Consequently, only the temporal layers are fine-tuned, while the spatial layers remain frozen. At each time step t , we concatenate the clean z_{ref} with the noisy latent z_t , which contains N frames, resulting in a latent representation with $(N + 1)$ frames as input. We then select only the last N frames from the denoised z_t .



Figure 3. Motion mask guidance examples. The first column and second column are the input mask and motion mask respectively. The user can specify one or multiple movable areas in the motion mask to fine grained control the video generation.

3.3. Motion Area Guidance

we introduce motion area guidance to provide users with precise control over the movable area of the input image. As shown in Figure 2, we concatenate the motion area mask with the video latent in the channel dimension. Drawing inspiration from ControlNet [63], we initialize the convolution kernel of the mask channel with zeros to maintain the original video generation capability.

We construct the training pairs of video and corresponding motion area masks from real videos using the following approach. Firstly, we convert the given video sample with N frames to gray-scale. Then, we calculate frame differences that exceed a threshold value T_m . These differences are then combined to create the difference binary mask d :

$$d = \bigcup_{i=1}^{N-1} (|x_{gray}^i - x_{gray}^{i-1}| > T_m), \quad (4)$$

where x_{gray}^i is the gray-scale of the i -th frame, the threshold T_m determines the intensity of motion in both movable and non-movable areas. If T_m is set too high, objects in non-movable areas may still appear to move. Conversely, if T_m is set too low, objects in non-movable areas might be completely frozen, potentially causing image artifacts near

the boundary of the motion area mask. Subsequently, we identify the contours of these difference areas in d and construct the motion area mask m by assigning label 1 to the pixels contained within these contours, indicating the movable area. Finally, considering the motion area mask m , we post-process the video latent z_0 such that pixels in the non-movable area are reset to the values of the first frame z_0^0 :

$$z'_0 = (1 - m) \cdot z_0^0 + m \cdot z_0. \quad (5)$$

We use z_t^i to denote the i -th frame of the video latent at time step t . As illustrated in Section 4.4, the post-processing step significantly enhances the effectiveness of the motion area guidance. To address subtle movements imperceptible to the human eye, which should not be marked as the movable area, we explicitly instruct the model to keep these pixels unchanged. The motion threshold T_m is adjusted to ensure that the visual differences between the reconstructed video z'_0 and z_0 remain reasonably small. The impact of motion area guidance on is demonstrated in Figure 3.

3.4. Motion Strength Guidance

During our training process, we observed that the sampling FPS affects the motion speed of the movable objects in the generated videos. However, using FPS alone as the

motion speed guidance for video generation is inadequate, as videos with the same FPS may exhibit varying motion speeds based on their content. Therefore, FPS alone cannot effectively regulate the speed of object motion. Consequently, we propose a metric called motion strength s to quantitatively measure the motion speed of the target motion area:

$$s(z) = \frac{1}{N-1} \sum_{i=1}^N |z^i - z^{i-1}|. \quad (6)$$

Here, the motion strength quantifies the differences between frames in the latent space. Similar to the time step, we project the motion strength into a positional embedding and add it to each frame in the residual block to ensure uniform application of the motion strength to every frame. The impact of motion strength guidance on the animation results is illustrated in Figure 4.

Training our motion strength guided pipeline directly with the noise prediction loss defined in Equation 3 is hard to converge. This is likely due to the fact that the noise prediction loss is primarily influenced by the frame-level image difference and does not directly supervise the inter-frame difference. Therefore, we introduce a motion strength loss to directly supervise the inter-frame difference:

$$l_s = \|s(z_0) - s(\hat{z}_0)\|_2^2, \quad (7)$$

where \hat{z}_0 represents the model’s estimated clean video latent z_0 , which can be obtained by transforming Equation 2 as:

$$\hat{z}_0 = \frac{z_0 - \sqrt{1 - \bar{\alpha}_t} \epsilon_\theta(z_t, t, c)}{\sqrt{\bar{\alpha}_t}}. \quad (8)$$

Finally, we combine the noise prediction loss and the motion strength loss with the scaling factor λ .

$$l = l_\epsilon + \lambda \cdot l_s. \quad (9)$$

3.5. Guidance Composition

Our image animation model integrates guidance from reference images, text, motion areas, and motion strength. During training, we vary the textual prompt and motion area to allow the model to accept different combinations of guidance during inference. However, conflicting guidance inputs can diminish their individual effects. For instance, if the text prompt does not align with the content of the reference image, the model prioritizes fidelity to the image. Fortunately, with motion area guidance, objects outside the motion area mask are completely frozen, allowing for interactive editing of the generated animation. As demonstrated in the last row of Figure 1, different objects can be animated with different texts.



Figure 4. Motion strength guidance examples. Augmenting the motion strength accelerates the alteration of Mona Lisa’s expression, but excessive motion strength may lead to the loss of fine-grained facial details.

3.6. Shared Noise Inference

During training, we construct the input latent by adding noise on the clean video latent. This noise schedule leaves some residual signal even at the terminal diffusion timestep T . As a consequence, the diffusion model fails to generalize faithful image animation during test time when we sample from random Gaussian noise without any real data signal. To solve this train-test discrepancy problem, during testing, we obtain the base noise by adding noise on z_{ref} using the forward process of DDPM [15]. As the DDPM independently samples random noise ϵ^i for each frame, it allows for frame diversity. The DDPM independently samples random noise ϵ^i for each frame, allowing for frame diversity. The noise latent for frame i can be expressed as:

$$z_T^i = \sqrt{\bar{\alpha}_T} z_{ref} + \sqrt{1 - \bar{\alpha}_T} \epsilon^i, \quad (10)$$

where $\bar{\alpha}_T$ denotes the diffusion factor. This approach combines the base noise with z_{ref} to achieve a balance between preserving the reference image information and introducing frame-specific diversity through the random noise ϵ^i . This design decision is critical for high image fidelity animation.

4. Experiment

4.1. Experimental Setup

Datasets. Our model is initialized from VideoComposer [22] which pretrains on WebVid10M [2]. Then we

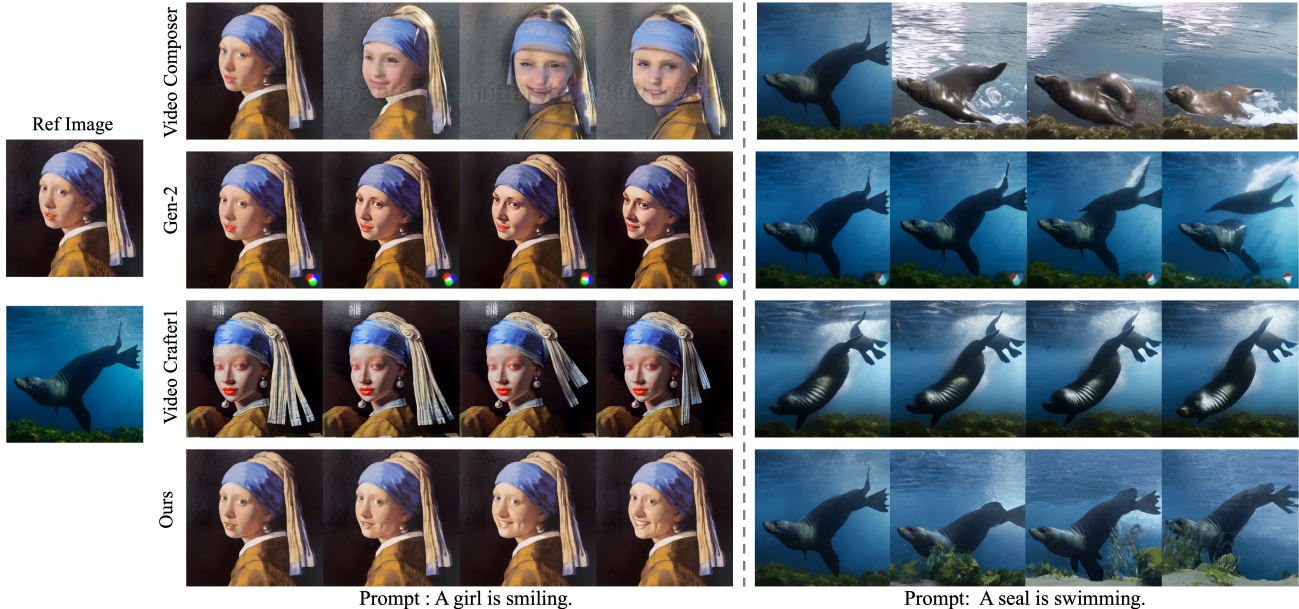


Figure 5. Qualitative Results. Comparing to open sourced methods Video Composer and VideoCrafter1, our method achieves higher image fidelity. Comparing to the commercial product Gen-2, our method achieves higher frame consistency.

finetune it on 20K videos randomly sampled from HD-VILA-100M [61] to remove watermark. Following [48, 51, 56], we conduct evaluation on MSR-VTT dataset [60] in a zero-shot setting. MSR-VTT is an open domain video retrieval dataset, where each video clip is accompanied by 20 natural sentences for description. Typically, the textual descriptions corresponding to the 2,990 video clips in its test set are utilized as prompts to generate videos.

Evaluation Metrics. Following previous methods [11, 48], we use Fréchet Video Distance (FVD) [50] to measure the video generation quality. We also use the Frame Consistency measured via CLIP cosine similarity of consecutive frames to show the temporal consistency of video. We propose the metric Motion Mask Precision to measure the effect of motion mask guidance, which calculates the percentage of the moving area of generated video within the given motion area mask. To measure the effect of motion strength guidance, we propose Motion Strength Error, which is the mean squared error of the generated video motion strength and the given video motion strength. In this section, all statistics are collected by generating 16-frame videos in 256×256 resolution with DDIM [49] algorithm in 50 steps.

Implements Details. We employ the AdamW [31] optimizer with a learning rate of 5×10^{-5} for training our model. All experiments are conducted on a single NVIDIA A10 GPU, requiring approximately 20 GB of vRAM for training and 6 GB of vRAM for inference. To enhance the model performance, we conduct multiple frame rate sampling during training, utilizing various frame rates (e.g., 4, 8, 12) to obtain an 8-frame training clip with a resolution of 384×384 . We train the model for 10,000 iterations with a

batch size of 2, which costs about 1 day. The motion area mask threshold T_m is set to 5 and the motion strength loss scaling factor λ is set to 0.001.

4.2. Quantitative Results

Table 1 presents the quantitative results of the zero-shot video generation ability on MSR-VTT compared to existing methods. To ensure a fair comparison, all models are evaluated on a resolution of 256×256 . With the same text and first frame condition, our method achieves lower FVD comparing to VideoComposer and concurrent work VideoCrafter1, which is evident that integrating fine-grained spatial information into the conditions leads to a significant improvement. This improvement suggests that our method is capable of generating more coherent videos than previous approaches.

Method	Conditions	Params(B)	FVD(↓)
CogVideo [19]	text	15.5	1294
LVDM [14]	text	1.16	742
MagicVideo [65]	text	-	998
VideoComposer [52]	text	1.85	580
VideoFusion [32]	text	1.83	581
ModelScope [51]	text	1.70	550
VideoComposer [52]	text&image	2.49	551
VideoCrafter1 [5]	text&image	3.24	465
Ours	text&image	1.81	443

Table 1. Video generation performance on the test set of MSR-VTT. “Conditions” denotes the type of condition for generation.

Method	FVD	Consistency	Time(s)	Mem(G)
CLIP Vision Global Token	551	0.879	22.13	11.1
CLIP Vision Full Tokens	457	0.911	24.12	11.7
Concat Latent Spatial	450	0.917	20.38	5.7
Concat Latent Temporal	443	0.916	21.54	5.9

Table 2. The performance comparison of image condition designs.

4.3. Qualitative Results

We present several visual examples of our method with three baselines: VideoComposer [52], Gen-2 [1] and VideoCrafter1 [5] in Figure 5. All the methods have the ability to generate videos based on reference image, thus showcasing the significant progress in image-conditioned video generation. VideoComposer and VideoCrafter1 achieves satisfactory levels of fluency but lost details of the reference image. In contrast, our proposed method preserves the latent representation of the first frame and denoises the subsequent frames, which plays a fundamental role in ensuring faithful video generation. Despite Gen-2’s relatively successful preservation of temporal consistency, it falls short in effectively controlling the motion amplitudes of the generated videos. In contrast, our method offers the flexibility of adjusting motion strength, where larger strengths correspond to greater motion amplitudes.

4.4. Ablation Study

Image condition We conduct an analysis of various design strategies for injecting reference image information in Table 2. The “CLIP Vision Global Token” method used by Video Composer [52] encodes the input image to vision tokens using CLIP image encoder and only injects the global [CLS] token into the U-Net through cross attention. The “CLIP Vision Full Tokens” method, used by VideoCrafter1 [5], projects and concatenates all vision tokens with the text embedding. As shown in Figure 5, CLIP vision tokens contain rich semantic information by pretraining on text and image pairs, but image details such as background texture and face details may be lost. Using all vision tokens also requires more computation cost to compute the cross attention between the latent and additional vision tokens. To preserve more image details, we first try the “Concat Latent Spatial” method, which concatenates the reference image latent from VAE with every frame on the channel dimension. However, we notice that this method limits the diversity of video motion when generating long videos. Finally, we concatenate the input image latent and the noise latent on the temporal dimension. As shown in “Concat Latent Temporal”, this method produces videos with better image fidelity and achieves better inference efficiency without using the additional ViT vision encoder.

Motion area guidance Table 3 illustrates different design choices for motion area guidance. A simple and training-

Method	Motion Mask Precision
No Control	0.21
Mask Guidance	0.52
Mask Guidance + Freeze	0.82

Table 3. Ablation study of the motion mask guidance. Our proposed strategy demonstrates effective capability in following designated motion areas to generate corresponding animation videos.

Method	Motion Strength Error
No Control	14.19
Adding Noise	12.74
FPS Guidance	8.37
Motion Strength Guidance	4.82
Motion Strength Guidance + Loss	2.36

Table 4. Ablate the design of the motion strength guidance. Comparing to FPS guidance, our method offers greater flexibility in incorporating motion into animation videos.

free approach to freeze the area outside the motion area is to apply the motion mask on the noise video latent, therefore the latent values outside motion area are to the same. However, this method produces videos nearly not moves, since the freeze noise latent is not Gaussian noise, which is inconsistent with the training setting. In Table 3, the “Mask Guidance” method concatenates the motion area mask and the noise latent as the input to the U-Net. “Mask Guidance + Freeze” is our proposed method that the latent values in non-movable areas are frozen and set to be the same as the first frame. We can observe the strategy of freezing non-movable areas helps the model to easily learn the guidance between the motion area mask and the target video.

Motion strength guidance We compare different design choices of motion strength guidance in Table 4. Since the initial noise video latent is generated by adding noise on z_{ref} , we can perform limited control over motion strength by the amount of added noise, as indicated by “Adding Noise”. The performance of FPS guidance is largely depend on the video content, so its variance is large. Comparing to FPS, our motion strength guidance performs more stable and achieve lower motion strength error.

5. Conclusion and Future Work

In this paper, we have presented an open domain image animation pipeline with a video diffusion model, incorporating motion area and motion strength guidance. While our method has shown promising results in achieving fine-grained and interactive image animation, it is important to acknowledge that our model has not been trained on high-resolution videos due to limited training resources. This limitation constrains the applicability and performance of our method in generating high-resolution animations.

References

- [1] Gen-2. Accessed October 22, 2023 [Online] <https://research.runwayml.com/gen2>. 8
- [2] Max Bain, Arsha Nagrani, Gul Varol, and Andrew Zisserman. Frozen in time: A joint video and image encoder for end-to-end retrieval. In *Proceedings of the IEEE/CVF International Conference on Computer Vision*, pages 1728–1738, 2021. 6
- [3] Hugo Bertiche, Niloy J Mitra, Kuldeep Kulkarni, Chun-Hao P Huang, Tuanfeng Y Wang, Meysam Madadi, Sergio Escalera, and Duygu Ceylan. Blowing in the wind: Cyclenet for human cinemagraphs from still images. In *CVPR*, 2023. 1, 3
- [4] Andreas Blattmann, Timo Milbich, Michael Dorkenwald, and Bjorn Ommer. Understanding object dynamics for interactive image-to-video synthesis. In *CVPR*, 2021. 1, 3
- [5] Haoxin Chen, Menghan Xia, Yin-Yin He, Yong Zhang, Xiaodong Cun, Shaoshu Yang, Jinbo Xing, Yaofang Liu, Qifeng Chen, Xintao Wang, Chao-Liang Weng, and Ying Shan. Videocrafter1: Open diffusion models for high-quality video generation. *ArXiv*, abs/2310.19512, 2023. 1, 3, 7, 8
- [6] Mark Chen, Alec Radford, Rewon Child, Jeffrey Wu, Heewoo Jun, David Luan, and Ilya Sutskever. Generative pre-training from pixels. In *International conference on machine learning*, pages 1691–1703. PMLR, 2020. 3
- [7] Chia-Chi Cheng, Hung-Yu Chen, and Wei-Chen Chiu. Time flies: Animating a still image with time-lapse video as reference. In *CVPR*, 2020. 1, 3
- [8] Yung-Yu Chuang, Dan B Goldman, Ke Colin Zheng, Brian Curless, David H Salesin, and Richard Szeliski. Animating pictures with stochastic motion textures. In *ACM SIGGRAPH*, 2005. 3
- [9] Yuki Endo, Yoshihiro Kanamori, and Shigeru Kuriyama. Animating landscape: self-supervised learning of decoupled motion and appearance for single-image video synthesis. *ACM TOG*, 38(6):1–19, 2019. 1
- [10] Patrick Esser, Robin Rombach, and Bjorn Ommer. Taming transformers for high-resolution image synthesis. In *Proceedings of the IEEE/CVF conference on computer vision and pattern recognition*, pages 12873–12883, 2021. 3
- [11] Patrick Esser, Johnathan Chiu, Parmida Atighehchian, Jonathan Granskog, and Anastasis Germanidis. Structure and content-guided video synthesis with diffusion models. In *Proceedings of the IEEE/CVF International Conference on Computer Vision*, pages 7346–7356, 2023. 1, 4, 7
- [12] Jiahao Geng, Tianjia Shao, Youyi Zheng, Yanlin Weng, and Kun Zhou. Warp-guided gans for single-photo facial animation. *ACM TOG*, 37(6):1–12, 2018. 1, 3
- [13] Ian Goodfellow, Jean Pouget-Abadie, Mehdi Mirza, Bing Xu, David Warde-Farley, Sherjil Ozair, Aaron Courville, and Yoshua Bengio. Generative adversarial networks. *Communications of the ACM*, 63(11):139–144, 2020. 3
- [14] Yingqing He, Tianyu Yang, Yong Zhang, Ying Shan, and Qifeng Chen. Latent video diffusion models for high-fidelity video generation with arbitrary lengths. *arXiv preprint arXiv:2211.13221*, 2022. 1, 7
- [15] Jonathan Ho, Ajay Jain, and Pieter Abbeel. Denoising diffusion probabilistic models. *Advances in neural information processing systems*, 33:6840–6851, 2020. 3, 6
- [16] Jonathan Ho, William Chan, Chitwan Saharia, Jay Whang, Ruiqi Gao, Alexey Gritsenko, Diederik P Kingma, Ben Poole, Mohammad Norouzi, David J Fleet, et al. Imagen video: High definition video generation with diffusion models. *arXiv preprint arXiv:2210.02303*, 2022. 3
- [17] Jonathan Ho, Tim Salimans, Alexey Gritsenko, William Chan, Mohammad Norouzi, and David J Fleet. Video diffusion models. In *NeurIPS*, 2022. 1, 3, 4
- [18] Aleksander Holynski, Brian L Curless, Steven M Seitz, and Richard Szeliski. Animating pictures with eulerian motion fields. In *CVPR*, 2021. 1, 3
- [19] Wenyi Hong, Ming Ding, Wendi Zheng, Xinghan Liu, and Jie Tang. Cogvideo: Large-scale pretraining for text-to-video generation via transformers. *arXiv preprint arXiv:2205.15868*, 2022. 7
- [20] Yaosi Hu, Chong Luo, and Zhenzhong Chen. Make it move: Controllable image-to-video generation with text descriptions. *2022 IEEE/CVF Conference on Computer Vision and Pattern Recognition (CVPR)*, pages 18198–18207, 2021. 3
- [21] Yaosi Hu, Chong Luo, and Zhenzhong Chen. Make it move: controllable image-to-video generation with text descriptions. In *CVPR*, 2022. 1
- [22] Lianghua Huang, Di Chen, Yu Liu, Yujun Shen, Deli Zhao, and Jingren Zhou. Composer: Creative and controllable image synthesis with composable conditions. *arXiv preprint arXiv:2302.09778*, 2023. 3, 6
- [23] Wei-Cih Jhou and Wen-Huang Cheng. Animating still landscape photographs through cloud motion creation. *IEEE TMM*, 18(1):4–13, 2015. 1, 3
- [24] Laurynas Karazija, Iro Laina, Andrea Vedaldi, and C. Rupprecht. Diffusion models for zero-shot open-vocabulary segmentation. *ArXiv*, abs/2306.09316, 2023. 4
- [25] Johanna Karras, Aleksander Holynski, Ting-Chun Wang, and Ira Kemelmacher-Shlizerman. Dreampose: Fashion image-to-video synthesis via stable diffusion. *arXiv preprint arXiv:2304.06025*, 2023. 1, 3
- [26] Levon Khachatryan, Andranik Movsisyan, Vahram Tadevosyan, Roberto Henschel, Zhangyang Wang, Shant Navasardyan, and Humphrey Shi. Text2video-zero: Text-to-image diffusion models are zero-shot video generators. *arXiv preprint arXiv:2303.13439*, 2023. 1, 3
- [27] Diederik P Kingma and Max Welling. Auto-encoding variational bayes. *arXiv preprint arXiv:1312.6114*, 2013. 2, 3
- [28] Xingyi Li, Zhiguo Cao, Huiqiang Sun, Jianming Zhang, Ke Xian, and Guo-Shing Lin. 3d cinemagraphy from a single image. *2023 IEEE/CVF Conference on Computer Vision and Pattern Recognition (CVPR)*, pages 4595–4605, 2023. 1, 3
- [29] Zhengqi Li, Richard Tucker, Noah Snaveley, and Aleksander Holynski. Generative image dynamics. *arXiv preprint arXiv:2309.07906*, 2023. 1, 3
- [30] Ziyi Li, Qinye Zhou, Xiaoyun Zhang, Ya Zhang, Yanfeng Wang, and Weidi Xie. Open-vocabulary object segmentation with diffusion models. 2023. 4

- [31] Ilya Loshchilov and Frank Hutter. Decoupled weight decay regularization. In *7th International Conference on Learning Representations, ICLR 2019*, 2019. 7
- [32] Zhengxiong Luo, Dayou Chen, Yingya Zhang, Yan Huang, Liang Wang, Yujun Shen, Deli Zhao, Jingren Zhou, and Tieniu Tan. Videofusion: Decomposed diffusion models for high-quality video generation. In *Proceedings of the IEEE/CVF Conference on Computer Vision and Pattern Recognition*, pages 10209–10218, 2023. 1, 7
- [33] Aniruddha Mahapatra and Kuldeep Kulkarni. Controllable animation of fluid elements in still images. In *CVPR*, 2022. 1, 3
- [34] Aniruddha Mahapatra, Aliaksandr Siarohin, Hsin-Ying Lee, S. Tulyakov, and Jun-Yan Zhu. Synthesizing artistic cinemagraphs from text. *ArXiv*, abs/2307.03190, 2023. 1, 3
- [35] Chong Mou, Xintao Wang, Liangbin Xie, Jian Zhang, Zhong-gang Qi, Ying Shan, and Xiaohu Qie. T2i-adapter: Learning adapters to dig out more controllable ability for text-to-image diffusion models. *arXiv preprint arXiv:2302.08453*, 2023. 3
- [36] Haomiao Ni, Changhao Shi, Kai Li, Sharon X Huang, and Martin Renqiang Min. Conditional image-to-video generation with latent flow diffusion models. In *Proceedings of the IEEE/CVF Conference on Computer Vision and Pattern Recognition*, pages 18444–18455, 2023. 3
- [37] Alex Nichol, Prafulla Dhariwal, Aditya Ramesh, Pranav Shyam, Pamela Mishkin, Bob McGrew, Ilya Sutskever, and Mark Chen. Glide: Towards photorealistic image generation and editing with text-guided diffusion models. *arXiv preprint arXiv:2112.10741*, 2021. 3
- [38] Makoto Okabe, Ken Anjyo, Takeo Igarashi, and Hans-Peter Seidel. Animating pictures of fluid using video examples. In *Comput. Graph. Forum*, pages 677–686, 2009. 1, 3
- [39] William Peebles and Saining Xie. Scalable diffusion models with transformers. In *Proceedings of the IEEE/CVF International Conference on Computer Vision*, pages 4195–4205, 2023. 3
- [40] Dustin Podell, Zion English, Kyle Lacey, Andreas Blattmann, Tim Dockhorn, Jonas Müller, Joe Penna, and Robin Rombach. Sdxl: improving latent diffusion models for high-resolution image synthesis. *arXiv preprint arXiv:2307.01952*, 2023. 3
- [41] Alec Radford, Jong Wook Kim, Chris Hallacy, Aditya Ramesh, Gabriel Goh, Sandhini Agarwal, Girish Sastry, Amanda Askell, Pamela Mishkin, Jack Clark, et al. Learning transferable visual models from natural language supervision. In *International conference on machine learning*, pages 8748–8763. PMLR, 2021. 2, 3, 4
- [42] Aditya Ramesh, Prafulla Dhariwal, Alex Nichol, Casey Chu, and Mark Chen. Hierarchical text-conditional image generation with clip latents, 2022. URL <https://arxiv.org/abs/2204.06125>, 7, 2022. 3
- [43] Robin Rombach, Andreas Blattmann, Dominik Lorenz, Patrick Esser, and Bjorn Ommer. High-resolution image synthesis with latent diffusion models. In *Proceedings of the IEEE/CVF conference on computer vision and pattern recognition*, pages 10684–10695, 2022. 3, 4
- [44] Olaf Ronneberger, Philipp Fischer, and Thomas Brox. U-net: Convolutional networks for biomedical image segmentation. In *Medical Image Computing and Computer-Assisted Intervention—MICCAI 2015: 18th International Conference, Munich, Germany, October 5-9, 2015, Proceedings, Part III 18*, pages 234–241. Springer, 2015. 3, 4
- [45] Chitwan Saharia, William Chan, Saurabh Saxena, Lala Li, Jay Whang, Emily L Denton, Kamyar Ghasemipour, Raphael Gontijo Lopes, Burcu Karagol Ayan, Tim Salimans, et al. Photorealistic text-to-image diffusion models with deep language understanding. *Advances in Neural Information Processing Systems*, 35:36479–36494, 2022. 3
- [46] Tamar Rott Shaham, Tali Dekel, and Tomer Michaeli. Singan: Learning a generative model from a single natural image. In *ICCV*, 2019. 1, 3
- [47] Aliaksandr Siarohin, Oliver J Woodford, Jian Ren, Menglei Chai, and Sergey Tulyakov. Motion representations for articulated animation. In *CVPR*, 2021. 1, 3
- [48] Uriel Singer, Adam Polyak, Thomas Hayes, Xi Yin, Jie An, Songyang Zhang, Qiyuan Hu, Harry Yang, Oron Ashual, Oran Gafni, et al. Make-a-video: Text-to-video generation without text-video data. *arXiv preprint arXiv:2209.14792*, 2022. 1, 3, 4, 7
- [49] Jiaming Song, Chenlin Meng, and Stefano Ermon. Denoising diffusion implicit models. In *ICLR*, 2021. 7
- [50] Thomas Unterthiner, Sjoerd van Steenkiste, Karol Kurach, Raphaël Marinier, Marcin Michalski, and Sylvain Gelly. Fvd: A new metric for video generation. 2019. 7
- [51] Jiuniu Wang, Hangjie Yuan, Dayou Chen, Yingya Zhang, Xiang Wang, and Shiwei Zhang. Modelscope text-to-video technical report. *arXiv preprint arXiv:2308.06571*, 2023. 7
- [52] Xiang Wang, Hangjie Yuan, Shiwei Zhang, Dayou Chen, Jiuniu Wang, Yingya Zhang, Yujun Shen, Deli Zhao, and Jingren Zhou. Videocomposer: Compositional video synthesis with motion controllability. *arXiv preprint arXiv:2306.02018*, 2023. 1, 3, 4, 7, 8
- [53] Yaohui Wang, Piotr Bilinski, Francois Bremond, and Antitza Dantcheva. Imaginator: Conditional spatio-temporal gan for video generation. 2020. 1, 3
- [54] Yaohui Wang, Di Yang, Francois Bremond, and Antitza Dantcheva. Latent image animator: Learning to animate images via latent space navigation. In *ICLR*, 2021. 1, 3
- [55] Chung-Yi Weng, Brian Curless, and Ira Kemelmacher-Shlizerman. Photo wake-up: 3d character animation from a single photo. In *CVPR*, 2019. 1, 3
- [56] Chenfei Wu, Jian Liang, Lei Ji, Fan Yang, Yuejian Fang, Daxin Jiang, and Nan Duan. Nüwa: Visual synthesis pre-training for neural visual world creation. In *European conference on computer vision*, pages 720–736. Springer, 2022. 7
- [57] Jay Zhangjie Wu, Yixiao Ge, Xintao Wang, Stan Weixian Lei, Yuchao Gu, Yufei Shi, Wynne Hsu, Ying Shan, Xiaohu Qie, and Mike Zheng Shou. Tune-a-video: One-shot tuning of image diffusion models for text-to-video generation. In *Proceedings of the IEEE/CVF International Conference on Computer Vision*, pages 7623–7633, 2023. 3

- [58] Wenpeng Xiao, Wentao Liu, Yitong Wang, Bernard Ghanem, and Bing Li. Automatic animation of hair blowing in still portrait photos. In *ICCV*, 2023. 1, 3
- [59] Wei Xiong, Wenhan Luo, Lin Ma, Wei Liu, and Jiebo Luo. Learning to generate time-lapse videos using multi-stage dynamic generative adversarial networks. In *CVPR*, 2018. 1, 3
- [60] Jun Xu, Tao Mei, Ting Yao, and Yong Rui. Msr-vtt: A large video description dataset for bridging video and language. In *Proceedings of the IEEE conference on computer vision and pattern recognition*, pages 5288–5296, 2016. 7
- [61] Hongwei Xue, Tiankai Hang, Yanhong Zeng, Yuchong Sun, Bei Liu, Huan Yang, Jianlong Fu, and Baining Guo. Advancing high-resolution video-language representation with large-scale video transcriptions. In *International Conference on Computer Vision and Pattern Recognition (CVPR)*, 2022. 7
- [62] Shengming Yin, Chenfei Wu, Jian Liang, Jie Shi, Houqiang Li, Gong Ming, and Nan Duan. Dragnuwa: Fine-grained control in video generation by integrating text, image, and trajectory. *arXiv preprint arXiv:2308.08089*, 2023. 3
- [63] Lvmin Zhang, Anyi Rao, and Maneesh Agrawala. Adding conditional control to text-to-image diffusion models. In *Proceedings of the IEEE/CVF International Conference on Computer Vision*, pages 3836–3847, 2023. 1, 3, 5
- [64] Yabo Zhang, Yuxiang Wei, Dongsheng Jiang, Xiaopeng Zhang, Wangmeng Zuo, and Qi Tian. Controlvideo: Training-free controllable text-to-video generation. *arXiv preprint arXiv:2305.13077*, 2023. 3
- [65] Daquan Zhou, Weimin Wang, Hanshu Yan, Weiwei Lv, Yizhe Zhu, and Jiashi Feng. Magicvideo: Efficient video generation with latent diffusion models. *arXiv preprint arXiv:2211.11018*, 2022. 1, 7